JOURNAL OF THE
ELECTRON DEVICES SOCIETY

Received 22 May 2021; revised 21 June 2021 and 26 July 2021; accepted 4 August 2021. Date of publication 10 August 2021;
date of current version 20 August 2021. The review of this article was arranged by Editor S. Reggiani.

Digital Object Identifier 10.1109/JEDS.2021.3103847

Analysis of Low Voltage RF Power Capability on AlGaN/GaN and InAlN/GaN HEMTs for Terminal Applications

**YUWEI ZHOU [1], JIEJIE ZHU [2], MINHAN MI [2], MENG ZHANG [2], PENGFEI WANG [2], YUTONG HAN [2],
SHENG WU [2], JIELONG LIU [1], QING ZHU [2], YILIN CHEN [1], BIN HOU [2],
XIAOHUA MA [2] (Member, IEEE), AND YUE HAO [2] (Senior Member, IEEE)**

1 School of Advanced Materials and Nanotechnology, Xidian University, Xi'an 710071, China
2 State Key Discipline Laboratory of Wide Band-Gap Semiconductor Technology, School of Microelectronics, Xidian University, Xi'an 710071, China

CORRESPONDING AUTHORS: X. MA AND M. MI (e-mail: xhma@xidian.edu.cn; miminhan@qq.com)

This work was supported in part by the National Key Research and Development Program of China under Grant 2020YFB1804902; in part by the National Natural Science Foundation of China under Grant 61904135; in part by the China Postdoctoral Science Foundation under Grant 2018M640957 and Grant BX20200262; in part by the Nature Science Foundation of Shaanxi Province under Grant 2020JQ-316; and in part by the Fundamental Research Funds for the Central Universities under Grant QTZX2172.

ABSTRACT In this work, low voltage RF power capability on AlGaN/GaN and InAlN/GaN HEMTs is analyzed from the perspective of DC and pulse characteristics, for terminal applications whose operating voltage is usually in the range of 3 to 15 V. Device fabrication is performed on mature AlGaN/GaN heterojunction as well as strongly polarized InAlN/GaN heterojunction, to make a comparison of low voltage RF power capability between two devices. Although it suffers from relatively severe RF dispersion, InAlN/GaN HEMT delivers higher output power density (P_{out}) than its opponent, benefiting from the lower parasitic resistance and knee voltage as well as higher output current density. At 8 GHz, P_{out} of 1.62 W/mm and 1.10 W/mm are achieved for InAlN/GaN and AlGaN/GaN HEMT, respectively, both of which are biased at class AB operation and V_{ds} of 9 V. However, the tremendous degradation of power added efficiency (PAE) occurs as the higher drain voltage is applied on InAlN/GaN HEMT, as the result of the severe gate leakage. What is more, a higher PAE is more necessary than P_{out} for terminal applications. Either InAlN/GaN HEMT or AlGaN/GaN HEMT has its own specific voltage range to deliver higher PAE. Concretely, InAlN/GaN HEMT is more suitable to applications with operating voltage not exceeding 6 V, and AlGaN/GaN HEMT is preferred for ones with relatively higher voltage, accompanied by the decent PAE as high as 62% to 66% and moderate P_{out} to meet the demand of various low voltage terminal applications.

INDEX TERMS AlGaN/GaN, InAlN/GaN, low voltage applications, RF power capability.

I. INTRODUCTION

Attributed to the advantages of wide bandgap, high electron velocity, large two-dimensional electron gas (2DEG) density, and high critical breakdown field, GaN-based HEMTs have been widely utilized in defense and civilian fields, such as radars, satellites, and macro base stations, where GaN HEMTs operate at high voltages to deliver high RF output power density (P_{out}) and power added efficiency (PAE) [1]–[3]. As for various mobile terminals, RF devices are required to operate at low to medium voltage levels from portable power supplies such as battery packs to provide high PAE and moderate P_{out} [4]. As is known, traditional GaAs technology has been employed in the terminal applications mentioned above. However, as a significant breakthrough, low voltage GaN technology is able to deliver higher PAE than GaAs technology at the same output power level to enable lower power consumption [5], exhibiting the application space of GaN technology could be expanded beyond the existing high voltage RF electronics to include low voltage ones [6], [7]. What's more, GaN technology has the superiority in bandwidth than GaAs technology, which makes it possible to realize high speed broadband communication as well as significant reduction in the number of power amplifier (PA), the chip area and the cost for mobile terminals. Consequently, GaN technology could be a strong competitor to GaAs technology in low voltage terminal applications.

To realize high performance GaN HEMTs at low voltage range, parasitic resistance consisting of contact resistance and access resistance ought to be reduced, so as to enhance P_{out} by increasing maximum output current density ($I_{d.max}$) and decreasing on-resistance (R_{on}) together with knee voltage (V_{knee}), and to improve PAE by diminishing Joule heat dissipation. What is particularly noteworthy is that enhanced P_{out} would be realized mainly via reducing parasitic resistance and suppressing RF dispersion in the premise of low operating voltages, which is different from the most commonly used method to improve P_{out} by increasing the operating voltage for high voltage GaN HEMTs. Moreover, off-state leakage current comprising buffer leakage current and reverse gate leakage current should also be suppressed to guarantee a sufficiently high breakdown voltage (at least two times the operating voltage) and maintain a low standby power consumption [8], [9].

The lower contact resistance could be achieved by optimization of RTA process [10], upgrade of ohmic metal schemes [11], [12], the recess of the barrier layer in the ohmic regions [13], [14], deposition of Ge and/or Si prior to ohmic metal evaporation [15], [16], and heavily doping in the ohmic regions by ion implantation or regrown ohmic contact [17], [18]. Additionally, scaling down the source-drain distance and adoption of strongly polarized high-Al-content heterojunction are meaningful to the reduction of access resistance [19]–[21]. Either dielectric deposition or plasma treatment is utilized in the access region and gate region to suppress RF dispersion and gate leakage current, respectively [22]–[26]. Besides, a sufficiently high aspect ratio should be maintained to strengthen the gate control and further diminish the buffer leakage current induced by DIBL.

Up to now, only a few researches on low voltage GaN HEMTs have been demonstrated, most of which are concerned with strongly polarized InAlN/GaN heterojunction [5]–[8]. And the low voltage RF power performance of AlGaN/GaN HEMT is rarely reported [4]. Moreover, the relation among DC characteristics, pulse characteristics, and RF power performance needs to be analyzed deeply and thoroughly. In this paper, device fabrication is performed on mature AlGaN/GaN heterojunction and low sheet resistance InAlN/GaN heterojunction, to make a comparison of low voltage RF power capability between two devices and find out the influence of multiple factors including parasitic resistance, Id.max, Vknee, RF dispersion, and gate leakage on low voltage RF power performance, which is helpful to guide the design of high performance low voltage GaN HEMTs in the future.

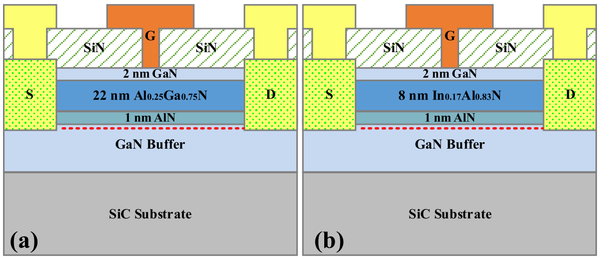

FIGURE 1. **Schematic cross sections of (a) AlGaN/GaN HEMT and (b) InAlN/GaN HEMT.**

II. DEVICE FABRICATION PROCESS

The schematic cross sections of AlGaN/GaN and InAlN/GaN HEMTs are shown in Fig. 1. The epilayers of both devices were grown on semi-insulating SiC substrates by metal organic chemical vapor deposition. The $Al_{0.25}$ $Ga_{0.75}$ N/GaN heterojunction comprised a 2-nm GaN cap, a 22-nm AlGaN barrier, a 1-nm AlN spacer, and a 1.3-μm GaN buffer. Room-temperature Hall measurement showed a 2DEG density of 0.86×10^{13} cm^{-2} and mobility of 1826 cm^2/V·s, leading to the sheet resistance (R_{sh}) of 398 $\Omega/\square$. The lattice-matched $In_{0.17}$ $Al_{0.83}$ N/GaN heterojunction consisted of a 2-nm GaN cap, an 8-nm InAlN barrier, a 1-nm AlN spacer, and a 1.3-μm GaN buffer. The density and mobility of 2DEG were 1.65×10^{13} cm^{-2} and 1512 cm^2/V·s, leading to the R_{sh} of 251 $\Omega/\square$, determined by Hall measurement at room-temperature.

Following device isolation by boron implantation, ohmic metals consisting of Ti/Al/Ni/Au stacks were deposited by electron beam evaporation. The AlGaN/GaN sample and InAlN/GaN sample were annealed in nitrogen ambient at 850°C for 30 s and 830°C for 30 s, respectively. The ohmic contact resistances were 0.46 and 0.28 Ω ·mm for two samples by using on-wafer transmission line measurement (TLM). The 120-nm SiN passivation layer was deposited at 250 °C by PECVD for both samples, and gate foot was defined by electron-beam lithography. Subsequently, gate foot was opened by CF_4-based plasma dry etching to remove SiN. Following gate head lithography, Ni/Au gate stacks were deposited by electron beam evaporation. Eventually, Ti/Au interconnection stacks were evaporated by electron beam evaporation after interconnection lithography. The T-shaped gate was formed with gate length of 0.2 μm and gate width of 2×50 μm. The source–drain spacing was 2 μm with gate–source spacing of 0.9 μm for both devices.

III. DEVICE CHARACTERISTICS AND DISCUSSION

A. DC CHARACTERISTICS

The Keithley 4200 semiconductor parameter analyzer was used for DC and pulsed I-V measurements. The comparison of transfer characteristics for both devices at V_{ds} of

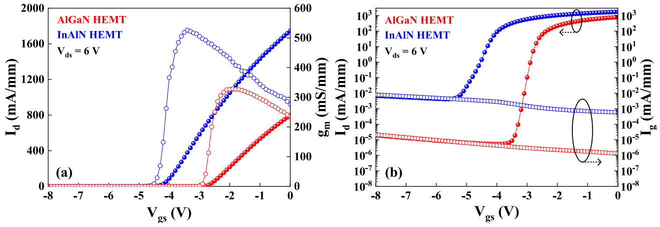

FIGURE 2. Comparison of transfer characteristics between AlGaN/GaN HEMT and InAlN/GaN HEMT on (a) the linear scale and (b) the semi-log scale at the drain voltage of 6 V.

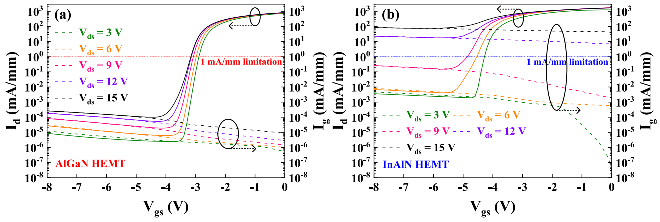

FIGURE 3. Transfer characteristics at five typical low drain voltages on the semi-log scale of (a) AlGaN/GaN and (b) InAlN/GaN HEMTs.

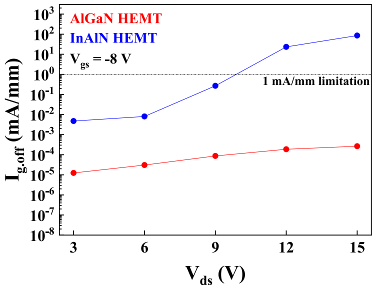

FIGURE 4. Influence of the operating voltage on the off-state gate leakage current for AlGaN/GaN and InAlN/GaN HEMTs.

6 V is shown in Fig. 2, exhibiting the peak extrinsic transconductance ($g_{m.peak}$) of 329 mS/mm and 526 mS/mm as well as the threshold voltage (V_{th}) of −2.9 V and −4.6 V for AlGaN/GaN and InAlN/GaN HEMTs, respectively. As demonstrated in Fig. 2 (b), the off-state drain leakage current ($I_{d.off}$) of InAlN/GaN HEMT is larger than that of AlGaN/GaN HEMT by 2 orders of magnitude, which would cause the terrible breakdown characteristics for InAlN/GaN HEMT. A higher on/off current ratio of 7 orders of magnitude is obtained for AlGaN/GaN HEMT, compared with that of 5 orders of magnitude for InAlN/GaN HEMT.

Further, the transfer characteristics of both devices at five typical low drain voltages are shown in Fig. 3 (a) and (b), to reveal the influence of the operating voltage on the off-state leakage current. It should be noted that PAE decreases with the larger reverse gate leakage current or off-state gate leakage current ($I_{g.off}$), and degrades dramatically once the $I_{g.off}$ threshold of about 1 mA/mm is reached [27]. Obviously, the off-state leakage current is dominated by reverse gate leakage current for both devices, leading to the $I_{d.off}$ is almost equal to the $I_{g.off}$. Overall, the $I_{g.off}$ increases with the larger drain voltage for both devices, as shown in Fig. 4.

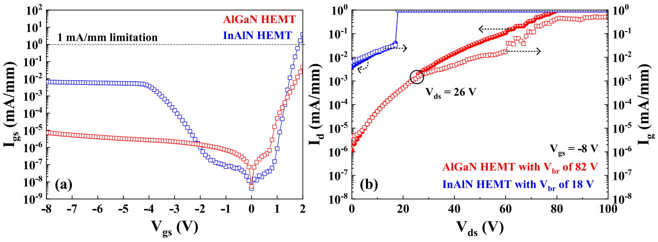

FIGURE 5. (a) Gate diode characteristics and (b) breakdown characteristics of AlGaN/GaN and InAlN/GaN HEMTs.

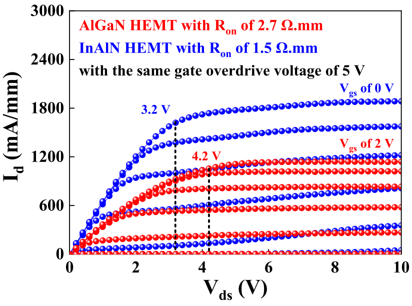

FIGURE 6. Output characteristics of AlGaN/GaN and InAlN/GaN HEMTs.

The $I_{g.off}$ increases slowly with the drain voltage and keeps within the range of 1×10^{-5} to 3×10^{-4} mA/mm for AlGaN/GaN HEMT, avoiding the potential PAE degradation. However, even if biased at the lower drain voltages below 6 V, InAlN/GaN HEMT suffers from the larger $I_{g.off}$ of 1×10^{-3} mA/mm magnitude. With the drain voltage exceeds 6 V, the $I_{g.off}$ degrades markedly and the $I_{g.off}$ threshold is reached as drain voltage is above 9 V, which implies the occurrence of severe PAE degradation.

Fig. 5 presents the gate diode characteristics and breakdown characteristics of InAlN/GaN and AlGaN/GaN HEMTs. As shown in Fig. 5 (a), the reverse gate leakage current of InAlN/GaN HEMT is larger than that of AlGaN/GaN HEMT by nearly 3 orders of magnitude, identical to the case of the off-state gate leakage current in Fig. 2 (b). The large gate leakage is attributed to the strong tunneling through the thin InAlN barrier [8]. In this paper, the breakdown voltage (V_{br}) is defined as the drain voltage where the drain current density reaches 1 mA/mm, while the device is biased at off-state. As demonstrated in Fig. 5 (b), the breakdown is caused by the severe gate leakage for InAlN/GaN HEMT with the V_{br} of 18 V, similar to the case in [8]. On the contrary, a decent V_{br} of 82 V is achieved for AlGaN/GaN HEMT due to rather low off-state leakage current. Additionally, the breakdown is caused by the combination of gate leakage and buffer leakage. Concretely, the off-state leakage current is dominated by reverse gate leakage current under the lower drain voltage not exceeding 26 V. However, the contribution of buffer leakage current increases with the higher drain voltage, ascribed to the poor 2DEG confinement.

Fig. 6 shows the output characteristics of both devices with the same gate overdrive voltage of 5 V, demonstrating

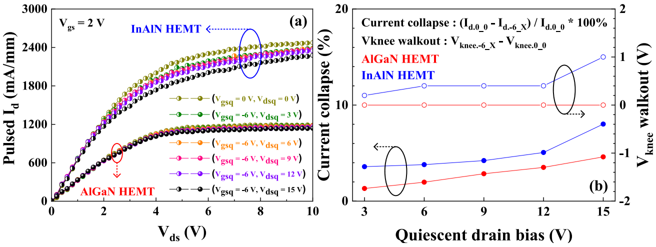

FIGURE 7. **(a) Pulsed I-V characteristics at the gate voltage of 2 V for AlGaN/GaN and InAlN/GaN HEMTs. (b) Current collapse and knee voltage walkout versus quiescent drain bias for both devices.**

the $I_{d.max}$ of 1140 mA/mm and 1884 mA/mm as well as the R_{on} of 2.7 Ω·mm and 1.5 Ω·mm for AlGaN/GaN HEMT and InAlN/GaN HEMT, respectively. Besides, a lower knee voltage of 3.2 V is obtained for InAlN/GaN HEMT, compared with that of 4.2 V for AlGaN/GaN HEMT. Better on-state characteristics with larger output current density and smaller on-resistance as well as lower knee voltage forebode higher P_{out} and PAE for InAlN/GaN HEMT.

B. PULSED I-V CHARACTERISTICS

Fig. 7 (a) shows the pulsed I-V measurements of AlGaN/GaN and InAlN/GaN HEMTs at the gate voltage of 2 V, with multiple low voltage quiescent bias points. It can be clearly seen that the RF dispersion is more serious in InAlN/GaN HEMT than AlGaN/GaN HEMT, as the result of relatively immature InAlN barrier crystalline quality. The current collapse and knee voltage walkout as a function of quiescent drain bias in the range of 3 to 15 V are summarized in Fig. 7 (b). In details, the current collapse ratio of AlGaN/GaN HEMT increases almost uniformly with the quiescent drain bias, and keeps below 4%. However, the current collapse ratio of InAlN/GaN HEMT increases relatively slowly until the quiescent drain bias is beyond 12 V. And the current collapse ratio of InAlN/GaN HEMT is always higher than that of AlGaN/GaN HEMT at the same quiescent drain bias. Besides, the knee voltage walkout value of AlGaN/GaN HEMT is a constant of zero indicating an ignorable knee voltage walkout, whereas that of InAlN/GaN HEMT increases with the quiescent drain bias and reaches as high as 1 V at the quiescent drain bias of 15 V. Similar to the current collapse, the knee voltage walkout value of InAlN/GaN HEMT is also always larger than that of AlGaN/GaN HEMT at the same bias. Both lower current collapse and ignorable knee voltage walkout are helpful to reach AlGaN/GaN HEMT's full potential in large signal characteristics. On the contrary, the RF power performance of InAlN/GaN HEMT would be discounted more.

Compared with AlGaN/GaN HEMT, the gate leakage and RF dispersion of InAlN/GaN HEMT fabricated in this work are relatively large, which would be suppressed in the following device fabrication. The gate leakage and RF dispersion of InAlN/GaN HEMTs fabricated by different organizations are compared in Table 1, revealing that the large gate leakage and RF dispersion are commonly seen and intrinsic weakness of the existing InAlN/GaN HEMTs.

TABLE 1. **The comparison of gate leakage and RF dispersion for InAlN/GaN HEMTs.**

Ref.	Organization	Year	Off-state gate leakage (mA/mm)	Current collapse ratio
[28]	III–V Laboratory	2010	/	6%
[29]	ETH	2010	3	/
[30]	Lille University of Science and Technology	2011	3.78×10^{-1}	16%
[24]	University of Notre Dame	2011	1	16%
[31]	MIT	2011	7	/
[32]	ETH	2011	4.4×10^{-3}	/
[16]	BAE Systems	2015	3×10^{-2}	/
[33]	NTU	2017	1	/
[34]	NTU	2018	3	15%
[35]	University of Delaware	2019	2.41×10^{-2}	/
[36]	Xidian University	2019	6×10^{-3}	4%
[37]	Cornell University	2020	3	/
This work	**Xidian University**	**2021**	$\mathbf{5 \times 10^{-3}}$	**8%**

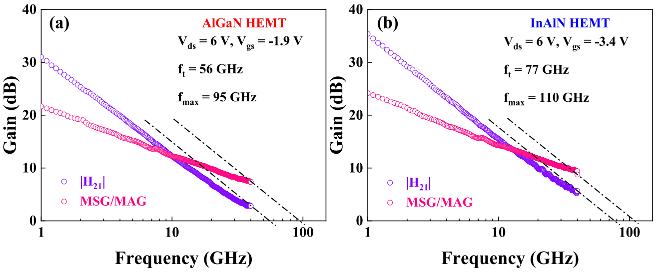

FIGURE 8. **Small signal characteristics of (a) AlGaN/GaN HEMT and (b) InAlN/GaN HEMT.**

C. RF POWER CHARACTERISTICS

S-parameters were measured in the frequency range of 1 to 40 GHz using Agilent 8363B vector network analyzer calibrated with a short-open through calibration standard. The bias points of (V_{gs}, V_{ds} = −1.9 V, 6 V) and (V_{gs}, V_{ds} = −3.4 V, 6 V) were chosen to achieve the optimal f_t/f_{max} for AlGaN/GaN and InAlN/GaN HEMTs, respectively. By extrapolating of the short circuit current gain ($|H_{21}|$) and the maximum stable gain/maximum available gain (MSG/MAG) curves using −20 dB/decade slopes, f_t/f_{max} values of 56/95 GHz and 77/110 GHz are obtained for AlGaN/GaN and InAlN/GaN HEMTs, respectively, shown in Fig. 8 (a) and (b). Higher f_t/f_{max} values of InAlN/GaN HEMT mainly derive from the lower parasitic resistance together with the higher transconductance.

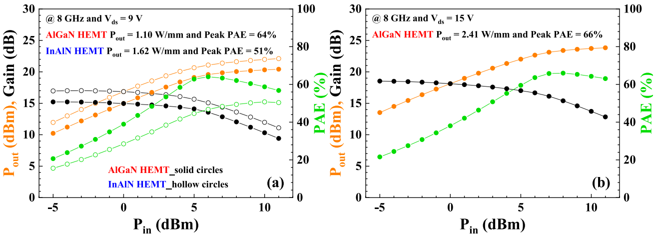

FIGURE 9. Large signal characteristics at 8 GHz of (a) AlGaN/GaN and InAlN/GaN HEMTs biased at the drain voltage of 9 V and (b) AlGaN/GaN HEMT biased at the drain voltage of 15 V.

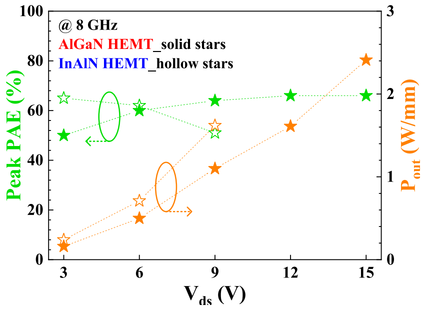

FIGURE 10. Output power density and power added efficiency versus low operating voltage at 8 GHz for AlGaN/GaN and InAlN/GaN HEMTs.

The low voltage RF power capability characterizations of AlGaN/GaN and InAlN/GaN HEMTs at 8 GHz were performed in continuous wave using an on-wafer load-pull system. Both the load and the source impedance were tuned for the optimum PAE. Fig. 9 shows the output power, the power gain, and the power added efficiency as a function of the input power for AlGaN/GaN and InAlN/GaN HEMTs, both of which were biased at class AB operation. As shown in Fig. 9 (a), P_{out} of 1.10 W/mm with PAE of 64% and P_{out} of 1.62 W/mm with PAE of 51% are achieved for AlGaN/GaN and InAlN/GaN HEMTs biased at V_{ds} of 9 V, respectively. Limited by the lower breakdown voltage of 18 V, InAlN/GaN HEMT could be characterized not exceeding 9 V [8], while AlGaN/GaN HEMT would be measured at higher voltages. At V_{ds} of 15 V, the PAE as high as 66% is achieved associated with P_{out} of 2.41 W/mm for AlGaN/GaN HEMT, as demonstrated in Fig. 9 (b).

Output power density and power added efficiency as a function of typical low operating voltage for AlGaN/GaN and InAlN/GaN HEMTs are summarized in Fig. 10. The P_{out} increases with the drain voltage for both devices, benefiting from increased drain voltage dynamic range and relatively weak RF dispersion. Within the drain voltage range of 3 to 9 V, the P_{out} of InAlN/GaN HEMT is always higher than that of AlGaN/GaN HEMT, which attributes to higher $I_{d.max}$ and lower V_{knee} as the result of lower parasitic resistance, in spite of the relatively larger current collapse and knee voltage walkout for InAlN/GaN HEMT, as shown in Fig. 7.

Benefiting from the lower parasitic resistance, InAlN/GaN HEMT delivers a 15% higher PAE than AlGaN/GaN HEMT at the same operating voltage of 3 V. Due to the slight increase in off-state gate leakage current from 5×10^{-3} mA/mm ($V_{ds} = 3$ V) to 8×10^{-3} mA/mm ($V_{ds} = 6$ V), as shown in Fig. 4, the PAE of InAlN/GaN HEMT decreases from 65% to 62%. Meanwhile, there is a large improvement in PAE from 50% to 60% for AlGaN/GaN HEMT, deriving from the increased drain voltage dynamic range. As a consequence, the superiority of InAlN/GaN HEMT in PAE is weakened at V_{ds} of 6 V. At V_{ds} of 9 V, the off-state gate leakage current increases significantly from 8×10^{-3} mA/mm to 3×10^{-1} mA/mm in a degree of 38 times higher, which leads to the large reduction in PAE to 51% for InAlN/GaN HEMT, much lower than the PAE of 64% for its competitor. Limited by the poor breakdown characteristics, InAlN/GaN HEMT cannot be measured at higher drain voltages above 9 V. Even if InAlN/GaN HEMT could be characterized at 12 V or 15 V, the off-state gate leakage current has been 23 mA/mm or 85 mA/mm beyond the threshold of 1 mA/mm, which would be accompanied by the huge PAE degradation according to [27]. Whereas, the PAE of AlGaN/GaN HEMT increases continuously with the drain voltage and maintains at 66% for V_{ds} exceeding 9 V.

By comparing the DC, pulsed I-V, and RF power characteristics between AlGaN/GaN HEMT and InAlN/GaN HEMT, it is found that a lower parasitic resistance together with an acceptable RF dispersion plays an important role in delivering a higher output power and power added efficiency. Different from the above positive factors, a larger gate leakage has a serious effect on PAE, especially for the strongly polarized high-Al-content heterojunctions which usually suffer from the severe gate leakage. In summary, InAlN/GaN HEMT has the advantage in delivering a higher P_{out} over AlGaN/GaN HEMT, attributed to the larger output current density and smaller on-resistance as well as lower knee voltage as the result of the lower parasitic resistance, regardless of the relatively larger but acceptable RF dispersion. However, the gate leakage becomes more severe as the higher drain voltage is applied on InAlN/GaN HEMT, giving rise to the increasing PAE degradation. As a result, the superiority of InAlN/GaN HEMT in PAE is weakened gradually with the higher voltages. For low voltage RF applications, a higher PAE is more attractive than P_{out}, and the P_{out} required is at the milliwatt (mW) level which could be easily satisfied by our devices with gate width of 100 μm. From the perspective of high PAE, InAlN/GaN HEMT is more popular with applications with operating voltage not exceeding 6 V, but is surpassed by AlGaN/GaN HEMT as operating voltage is over 6 V. To achieve low voltage GaN HEMTs with extremely high PAE for terminal applications, device fabrication should be performed on strongly polarized InAlN/GaN heterojunction. And the source–drain distance ought to be reduced as largely as possible. Besides, a lower contact resistance is in demand, which could be satisfied by advanced regrown ohmic contact process. Then, the RF dispersion should also be reduced, which can be realized by adjustment of the growth process of InAlN/GaN heterojunction to decrease the surface and bulk traps, optimization of the passivation process, or adoption of the field-plate structure to change the distribution of electric field. Most important of all, the large gate leakage is supposed to be suppressed by either dielectric deposition or plasma treatment under the gate.

IV. CONCLUSION

In this paper, AlGaN/GaN and InAlN/GaN HEMTs have been fabricated to reveal their low voltage RF power capability for terminal applications and make a comparison of the capability between each other. What is more, the low voltage RF power characteristics are investigated from the point of view of parasitic resistance, $I_{d.max}$, V_{knee}, RF dispersion, and gate leakage, which is useful for guiding the design of high performance low voltage GaN HEMTs in the days to come. Compared with InAlN/GaN HEMT, AlGaN/GaN HEMT has a negligible RF dispersion which is beneficial to reach AlGaN/GaN HEMT's full potential in large signal characteristics, but larger parasitic resistance and knee voltage as well as lower output current density leading to the lower P_{out}. Despite the advantage of higher P_{out}, InAlN/GaN HEMT suffers from the huge degradation of PAE at higher drain voltages, ascribed to the more severe gate leakage. Usually, a higher PAE is more significant than P_{out} to low voltage terminal applications, and not only InAlN/GaN HEMT but also AlGaN/GaN HEMT has its own specific voltage range to deliver higher PAE. In details, InAlN/GaN HEMT is fit for applications with operating voltages not exceeding 6 V, and AlGaN/GaN HEMT is more popular with applications with relatively higher voltages.

REFERENCES

[1] Y.-F. Wu, M. Moore, A. Saxler, T. Wisleder, and P. Parikh, "40-W/mm double field-plated GaN HEMTs," in *Proc. 64th Device Res. Conf.*, State College, PA, USA, 2006, pp. 151–152, doi: 10.1109/DRC.2006.305162.

[2] K. Osawa, H. Yoshikoshi, A. Nitta, T. Tanaka, E. Mitani, and T. Satoh, "Over 74% efficiency, L-band 200W GaN-HEMT for space applications," in *Proc. 46th Eur. Microw. Conf. (EuMC)*, London, U.K., 2016, pp. 397–400, doi: 10.1109/EuMC.2016.7824363.

[3] S. Nakajima, "GaN HEMTs for 5G base station applications," in *Proc. IEEE Int. Electron Devices Meeting (IEDM)*, San Francisco, CA, USA, 2018, pp. 14.2.1–14.2.4, doi: 10.1109/IEDM.2018.8614588.

[4] Z. Y. Zheng *et al.*, "GaN HEMT with convergent channel for low intrinsic knee voltage," *IEEE Electron Device Lett.*, vol. 41, no. 9, pp. 1304–1307, Sep. 2020, doi: 10.1109/led.2020.3010810.

[5] H. W. Then *et al.*, "High-performance low-leakage enhancement-mode high-K dielectric GaN MOSHEMTs for energy-efficient, compact voltage regulators and RF power amplifiers for low-power mobile SoCs," in *Proc. Symp. VLSI Technol. (VLSI Technology)*, Kyoto, Japan, 2015, pp. T202–T203, doi: 10.1109/VLSIT.2015.7223674.

[6] H. W. Then *et al.*, "3D heterogeneous integration of high performance high-K metal gate GaN NMOS and Si PMOS transistors on 300mm high-resistivity Si substrate for energy-efficient and compact power delivery, RF (5G and beyond) and SoC applications," in *Proc. IEEE Int. Electron Devices Meeting (IEDM)*, San Francisco, CA, USA, 2019, pp. 17.3.1–17.3.4, doi: 10.1109/IEDM19573.2019.8993583.

[7] H. W. Then *et al.*, "Gallium nitride and silicon transistors on 300 mm silicon wafers enabled by 3-D monolithic heterogeneous integration," *IEEE Trans. Electron Devices*, vol. 67, no. 12, pp. 5306–5314, Dec. 2020, doi: 10.1109/ted.2020.3034076.

[8] P. Saunier *et al.*, "InAlN barrier scaled devices for very high f_T and for low-voltage RF applications," *IEEE Trans. Electron Devices*, vol. 60, no. 10, pp. 3099–3104, Oct. 2013, doi: 10.1109/ted.2013.2277772.

[9] Z. H. Feng *et al.*, "18-GHz 3.65-W/mm enhancement-mode AlGaN/GaN HFET using fluorine plasma ion implantation," *IEEE Electron Device Lett.*, vol. 31, no. 12, pp. 1386–1388, Dec. 2010, doi: 10.1109/led.2010.2072901.

[10] Q. Feng, L. M. Li, Y. Hao, J. Y. Ni, and J. C. Zhang, "The improvement of ohmic contact of Ti/Al/Ni/Au to AlGaN/GaN HEMT by multi-step annealing method," *Solid-State Electron.*, vol. 53, no. 9, pp. 955–958, Jun. 2009, doi: 10.1016/j.sse.2009.06.002.

[11] L. Wang, F. M. Mohammed, and I. Adesida, "Differences in the reaction kinetics and contact formation mechanisms of annealed Ti/Al/Mo/Au Ohmic contacts on n-GaN and AlGaN/GaN epilayers," *J. Appl. Phys.*, vol. 101, no. 1, Jan. 2007, Art. no. 013702, doi: 10.1063/1.2402791.

[12] H. Sun *et al.*, "Optimization of Au-free ohmic contact based on the gate-first double-metal AlGaN/GaN MIS-HEMTs and SBDs process," *IEEE Trans. Electron Devices*, vol. 65, no. 2, pp. 622–628, Feb. 2018, doi: 10.1109/ted.2017.2778072.

[13] Y. Lu *et al.*, "High RF performance AlGaN/GaN HEMT fabricated by recess-arrayed ohmic contact technology," *IEEE Electron Device Lett.*, vol. 39, no. 6, pp. 811–814, Jun. 2018, doi: 10.1109/led.2018.2828860.

[14] B. Benakaprasad, A. M. Eblabla, X. Li, K. G. Crawford, and K. Elgaid, "Optimization of ohmic contact for AlGaN/GaN HEMT on low-resistivity silicon," *IEEE Trans. Electron Devices*, vol. 67, no. 3, pp. 863–868, Mar. 2020, doi: 10.1109/ted.2020.2968186.

[15] D. S. Lee, X. Gao, S. P. Guo, D. Kopp, P. Fay, and T. Palacios, "300-GHz InAlN/GaN HEMTs with InGaN back barrier," *IEEE Electron Device Lett.*, vol. 32, no. 11, pp. 1525–1527, Nov. 2011, doi: 10.1109/led.2011.2164613.

[16] D. Xu *et al.*, "0.1-µm atomic layer deposition Al_2O_3 passivated InAlN/GaN high electron-mobility transistors for E-band power amplifiers," *IEEE Electron Device Lett.*, vol. 36, no. 5, pp. 442–444, May 2015, doi: 10.1109/led.2015.2409264.

[17] T. Nanjo *et al.*, "Enhancement of drain current by an AlN spacer layer insertion in AlGaN/GaN high-electron-mobility transistors with Si-Ion-implanted source/drain contacts," *Jpn. J. Appl. Phys.*, vol. 50, no. 6, Jun. 2011, Art. no. 064101, doi: 10.1143/jjap.50.064101.

[18] J. Guo *et al.*, "MBE-regrown ohmics in InAlN HEMTs with a regrowth interface resistance of 0.05 Ω·mm," *IEEE Electron Device Lett.*, vol. 33, no. 4, pp. 525–527, Apr. 2012, doi: 10.1109/led.2012.2186116.

[19] K. Shinohara *et al.*, "Scaling of GaN HEMTs and schottky diodes for submillimeter-wave MMIC applications," *IEEE Trans. Electron Devices*, vol. 60, no. 10, pp. 2982–2996, Oct. 2013, doi: 10.1109/ted.2013.2268160.

[20] Y. Z. Yue *et al.*, "Ultrascaled InAlN/GaN high electron mobility transistors with cutoff frequency of 400 GHz," *Jpn. J. Appl. Phys.*, vol. 52, no. 8S, May 2013, Art. no. 08jn14, doi: 10.7567/jjap.52.08jn14.

[21] J. Green *et al.*, "ScAlN/GaN high-electron-mobility transistors with 2.4-A/mm current density and 0.67-S/mm transconductance," *IEEE Electron Device Lett.*, vol. 40, no. 7, pp. 1056–1059, Jul. 2019, doi: 10.1109/led.2019.2915555.

[22] D. Xu *et al.*, "0.1-µm InAlN/GaN high electron-mobility transistors for power amplifiers operating at 71–76 and 81–86 GHz: Impact of passivation and gate recess," *IEEE Trans. Electron Devices*, vol. 63, no. 8, pp. 3076–3083, Aug. 2016, doi: 10.1109/ted.2016.2579160.

[23] W. C. Xing, Z. H. Liu, K. Ranjan, G. I. Ng, and T. Palacios, "Planar nanostrip-channel Al_2O_3/InAlN/GaN MISHEMTs on Si with improved linearity," *IEEE Electron Device Lett.*, vol. 39, no. 7, pp. 947–950, Jul. 2018, doi: 10.1109/led.2018.2837886.

[24] R. H. Wang *et al.*, "210-GHz InAlN/GaN HEMTs with dielectric-free passivation," *IEEE Electron Device Lett.*, vol. 32, no. 7, pp. 892–894, Jul. 2011, doi: 10.1109/led.2011.2147753.

[25] M. H. Mi *et al.*, "Millimeter-wave power AlGaN/GaN HEMT using surface plasma treatment of access region," *IEEE Trans. Electron Devices*, vol. 64, no. 12, pp. 4875–4881, Dec. 2017, doi: 10.1109/ted.2017.2761766.

[26] M. H. Mi *et al.*, "90 nm gate length enhancement-mode AlGaN/GaN HEMTs with plasma oxidation technology for high-frequency application," *Appl. Phys. Lett.*, vol. 111, no. 17, Oct. 2017, Art. no. 173502, doi: 10.1063/1.5008731.

[27] J. L. Jimenez and U. Chowdhury, "X-band GaN FET reliability," in *Proc. IEEE Int. Rel. Phys. Symp.*, Phoenix, AZ, USA, 2008, pp. 429–435, doi: 10.1109/RELPHY.2008.4558923.

[28] N. Sarazin *et al.*, "AlInN/AlN/GaN HEMT technology on SiC With 10-W/mm and 50% PAE at 10 GHz," *IEEE Electron Device Lett.*, vol. 31, no. 1, pp. 11–13, Jan. 2010, doi: 10.1109/led.2009.2035145.

[29] H. F. Sun *et al.*, "100-nm-gate (Al,In)N/GaN HEMTs grown on SiC with F_T = 144GHz," *IEEE Electron Device Lett.*, vol. 31, no. 4, pp. 293–295, Apr. 2010, doi: 10.1109/led.2009.2039845.

[30] F. Lecourt *et al.*, "InAlN/GaN HEMTs on sapphire substrate with 2.9-W/mm output power density at 18 GHz," *IEEE Electron Device Lett.*, vol. 32, no. 11, pp. 1537–1539, Nov. 2011, doi: 10.1109/led.2011.2166949.

[31] D. S. Lee *et al.*, "245-GHz InAlN/GaN HEMTs with oxygen plasma treatment," *IEEE Electron Device Lett.*, vol. 32, no. 6, pp. 755–757, Jun. 2011, doi: 10.1109/led.2011.2132751.

[32] S. Tirelli, D. Marti, H. F. Sun, A. R. Alt, J. F. Carlin, N. Grandjean, and C. R. Bolognesi, "Fully passivated AlInN/GaN HEMTs with f_T/f_{MAX} of 205/220 GHz," *IEEE Electron Device Lett.*, vol. 32, no. 10, pp. 1364–1366, Oct. 2011, doi: 10.1109/led.2011.2162087.

[33] W. C. Xing, Z. H. Liu, H. D. Qiu, G. I. Ng, and T. Palacios, "Planar-nanostrip-channel InAlN/GaN HEMTs on Si with improved g_m and f_T linearity," *IEEE Electron Device Lett.*, vol. 38, no. 5, pp. 619–622, May 2017, doi: 10.1109/led.2017.2689810.

[34] W. C. Xing *et al.*, "InAlN/GaN HEMTs on Si with high f_T of 250 GHz," *IEEE Electron Device Lett.*, vol. 39, no. 1, pp. 75–78, Jan. 2018, doi: 10.1109/led.2017.2773054.

[35] P. Cui *et al.*, "High-performance InAlN/GaN HEMTs on silicon substrate with high $f_T \times L_g$," *Appl. Phys. Exp.*, vol. 12, no. 10, Aug. 2019, Art. no. 104001, doi: 10.7567/1882-0786/ab3e29.

[36] M. H. Mi *et al.*, "Improving the transconductance flatness of InAlN/GaN HEMT by modulating V_T along the gate width," *Appl. Phys. Exp.*, vol. 12, no. 11, Sep. 2019, Art. no. 114001, doi: 10.7567/1882-0786/ab48bf.

[37] L. Li *et al.*, "GaN HEMTs on Si with regrown contacts and cutoff/maximum oscillation frequencies of 250/204 GHz," *IEEE Electron Device Lett.*, vol. 41, no. 5, pp. 689–692, May 2020, doi: 10.1109/led.2020.2984727.